2013 IEEE/RSJ International Conference on
Intelligent Robots and Systems (IROS)
November 3-7, 2013. Tokyo, Japan

Control Allocation of All-Wheel Drive Vehicles: a Longitudinal Model

Asher Stern and Zvi Shiller

Abstract— **This paper offers a method to compute the control inputs for an all-wheel drive vehicle that moves along a specified path on rough terrain. The focus of this paper is on longitudinal motion only, using a half-car model with no suspensions. For a given path, we first compute the range of the admissible speeds and accelerations at every point along the path, subject to vehicle dynamics and constraints on the wheel/ground forces. A feasible velocity profile along the path is then computed to respect the admissible speeds and accelerations and satisfy given boundary conditions. While the velocity profile represents the accelerations of the center of mass, it remains to determine the control inputs (torques) for the two independent wheels. The challenge stems from the longitudinal model being an indeterminate system, having two control inputs but only one degree-of-freedom along the specified path. This inherent indeterminacy is resolved by adding a virtual suspension to the rigid vehicle model, which allows to explicitly compute the two individual wheel torques. The method is demonstrated for a vehicle moving at the time optimal speeds over a bump. A dynamic simulation of the vehicle with a stiff suspension shows that the two wheels maintain contact with the ground at all times, despite moving at the ultimate speeds. It is also shown that the all-wheel-drive model produces a larger set of admissible speeds and accelerations, and hence results in faster speeds and shorter motion times than the single drive (front or rear) model.**

I. Introduction

One advantage of electric vehicles is that they can be actuated at the wheels by individual hub motors [4], thus allowing individual control of each wheel (all-wheel-drive) for better stability and performance [8]. The main challenge in the control of hub motors is the determination of the control inputs to the individual wheels, while ensuring vehicle's stability at high speeds. Computing the individual control inputs for specified velocity profiles along specified paths over rough terrain for an all-wheel-drive longitudinal vehicle model is the focus of this paper. We choose to follow the time optimal velocity profile, which represents the ultimate vehicle speeds that ensure vehicle stability.

The computation of the ultimate speeds that ensures vehicle stability was treated earlier [10], [11]. It consists of projecting the vehicle's motion onto path coordinates and computing the velocity and acceleration limits along the path. The remaining challenge is to determine the individual wheel torques that generate this velocity profile and ensure vehicle stability. In the context of this paper, stability implies contact between all wheels and ground at all times. Moving at speeds that may cause the vehicle to be airborne is considered unsafe for autonomous vehicles and is therefore out of the scope of this paper.

The all-wheel drive model makes the computation of the individual wheel torques difficult since the vehicle model is indeterminate (more control inputs than degrees-of-freedom). We first solve this problem for a longitudinal vehicle model, with two controlled wheels. If the vehicle is moving along a specified path, its motion has only one DOF, whereas it is driven by two control inputs. The system is therefore indeterminate and over actuated.

A few solutions to the control of over actuated systems have been developed [7]. One approach, used to control lateral motion, closes the loop around each wheel to regulate some nominal state, such as speed [3], slip [2], [12] and motor current [15]. A similar approach was used for longitudinal motion of a half-car model [5], [6].

Another approach is Daisy Chaining, where the control signal is first computed for one actuator (for a one degree-of-freedom system), then the second actuator is used to compensate for the remaining error between the actual and desired acceleration [1]. While these approaches eliminate the need to explicitly compute the nominal motor torques, they cannot drive a vehicle along its performance envelope because of the control authority needed by the closed loop control. Another approach computes the control signals by minimizing the error between the desired and the actual acceleration produced by the wheel torques, using quadratic programming and accounting for ground force and motor constraints for [14] [9]. These approaches either do not produce the desired acceleration [3], [2], [12], [15], [1] or are computationally too intensive [14], [9].

This paper treats the control allocation problem for an all-wheel-drive vehicle that is moving along a specified path at a specified velocity profile. The speed profile is determined to ensure that it does not violate any force and control constraints. The wheel torques are computed by solving the inverse dynamics problem for the indeterminate system. This in turn is done by introducing a virtual suspension, which effectively reduces the number of unknown forces and thus allows a closed form solution for the actuator torques at each time step. The computation of the wheel torques is direct and hence computationally efficient. If the velocity profile used as the reference input is time optimal, then this approach would produce the time optimal wheel torques.

This approach is demonstrated for a half-car vehicle model moving over rough terrain at the time optimal speeds. A dynamic simulation of a similar vehicle model but having a stiff suspensions shows that despite the ultimate speeds, the two wheels maintain contact with the ground at all times. It

The authors are with the Paslin Robotics Research Laboratory, Department of Mechanical Engineering and Mechatronics, Ariel University, Ariel 40700, Israel. shiller@ariel.ac.il

is shown that the all-wheel-drive model produces a larger set of admissible speeds and accelerations, and hence results in faster speeds and shorter motion times than the single drive (front or rear) model.

II. Vehicle Model

This paper focuses on the planar vehicle shown in Figure 1. It consists of a rigid body of mass m and moment of inertia I that is driven by two actuated mass-less wheels of radius R. The forces acting on each wheel are the normal force F_n in the direction of the normal n to the ground and the traction force F_t in the direction of the tangent vector t at the point of contact. The traction force $F_t = TR$ is in effect the driving force, produced by the wheel torque T.

The vehicle's position is represented by the position (X,Z) of its center of mass and orientation θ in the the inertial frame. The back and front contact points are r_1 and r_2, respectively, relative to the center of mass, as shown in Figure 1.

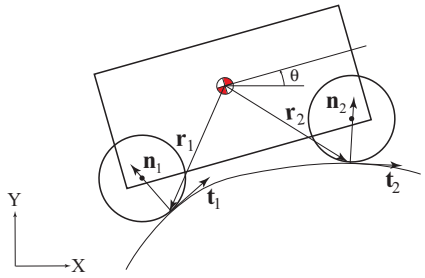

Fig. 1. A planar vehicle model

A. Kinematics

For a given terrain profile $f(X) \in \mathbb{R}$ and a given rear contact point $X_1 \in \mathbb{R}$, we need to compute the contact point, $X_2 \in \mathbb{R}$, of the front wheel. This in turn will yield the location of the center of mass x and the vehicle orientation θ. This is computed numerically by modeling the wheel center and the contact points as a closed kinematic chain [11].

By following a specified path, the vehicle has one degree-of-freedom, which can be represented by the arc length, $s \in \mathbb{R}$, of the trajectory followed by the center of mass. The vehicle's linear and angular acceleration are thus expressed in terms of the speed $\dot{s}$ and acceleration $\ddot{s}$ along the path. The acceleration $\ddot{x} \in \mathbb{R}^2$ can be expressed in terms of $\dot{s}$ and $\ddot{s}$ [11]:

$$\ddot{x} = x_s \ddot{s} + x_{ss} \dot{s}^2, \tag{1}$$

where x_s and x_{ss} are the 1^{st} and 2^{nd} derivatives of x with respect to s. .

The angular acceleration may be similarly expressed as:

$$\ddot{\theta} = \theta_s \ddot{s} + \theta_{ss} \dot{s}^2, \tag{2}$$

where θ_s and θ_{ss} are the 1^{st} and 2^{nd} derivatives of $\theta \in \mathbb{R}$ with respect to s.

B. Vehicle Dynamics

The equations of motion of the longitudinal vehicle consist of two force and one moment equations:

$$\begin{aligned} m\ddot{x} &= F_{t1}t_1 + F_{n1}n_1 + F_{t2}t_2 + F_{n2}n_2 + mg \qquad (3)\\ I\ddot{\theta} &= |r_1 \times (F_{t1}t_1 + F_{n1}n_1) + r_2 \times (F_{t2}t_2 + F_{n2}n_2)|, \end{aligned}$$

where $g \in \mathbb{R}^2$ is the gravity acceleration vector.

Substituting (1-2) in (3) yields:

$$\begin{aligned} m(x_s\ddot{s} + x_{ss}\dot{s}^2) &= F_{t1}t_1 + F_{n1}n_1 + F_{t2}t_2 + F_{n2}n_2 + mg \quad (4)\\ I(\theta_s\ddot{s} + \theta_{ss}\dot{s}^2) &= |r_1 \times (F_{t1}t_1 + F_{n1}n_1) + \\ &\qquad r_2 \times (F_{t2}t_2 + F_{n2}n_2)| \qquad (5) \end{aligned}$$

Equations (4) and (6) are driven by the two applied forces F_{t1} and F_{t2}. Their selection would determine the corresponding $\dot{s}$ and $\ddot{s}$. The constraints on F_{t1} and F_{t2}, derived from the friction constraints, thus map to constraints on $\dot{s}$ and $\ddot{s}$.

The ground forces of a typical wheel $i = 1,2$ are bounded by the friction constraints:

$$F_{ti} \leq \mu F_{ni} \tag{6}$$

$$F_{ti} \geq -\mu F_{ni} \tag{7}$$

Note that the vehicle is driven by two control inputs while its motion that maintains contact of the two wheels with the ground, is only of one degree-of-freedom. This can be seen by observing that by determining $s(t)$, one determines $\dot{s}$ and $\ddot{s}$. It is therefore impossible to directly compute the two control inputs for any given speed and acceleration along the path.

Furthermore, in addition to F_{t1} and F_{t2}, the equations of motion are also functions of the two normal forces F_{n1} and F_{n2}, which are unknown. In addition, the equations of motion are coupled since the right hand side of all three equations is a function of a common $\dot{s}$ and its derivative. The selection of proper control inputs is therefore not trivial.

Our approach to solving for the optimal control inputs consists of the following steps:

- determine the boundary of the set of feasible speeds and accelerations using the rigid body model (no suspension)
- compute the time optimal velocity profile (or any feasible velocity profile) along the path
- compute the two control inputs using a virtual suspension model, as discussed next.

III. The Set of Feasible Speeds and Accelerations

The set of feasible speeds and accelerations (FSA) is a convex polygon in the $\ddot{s} - \dot{s}^2$ plane, as shown schematically in Figure 2. It is formed by the intersection of four half planes, each satisfying two of the four inequality constraints (6)- (7) and the equations of motion (4) (6) [11]. The boundary of each half plane is determined by considering the equality part of the respective inequality constraints [11]. During motion,

the vehicle's speeds and accelerations must stay within FSA to ensure vehicle stability.

The right most point in this polygon indicates the maximum speed along the path, below which some acceleration exists so that none of the friction constraints (6)- (7) are violated. Plotting the maximum speed along the path forms the velocity limit curve, below which the time optimal velocity profile is computed [10].

The time optimal velocity profile along the path, computed using a previously developed algorithm [10], switches between the maximum acceleration and deceleration so as to avoid crossing the velocity limit curve. The details of this algorithm are beyond the scope of this paper.

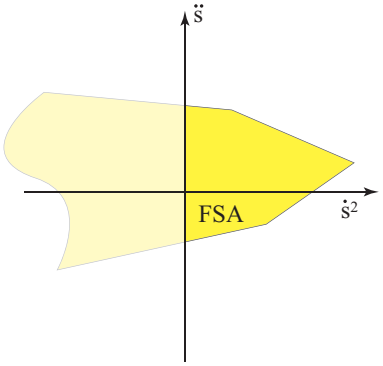

Fig. 2. The Feasible range of Speed and Acceleration (FSA).

IV. The Suspension Model

The one degree-of-freedom motion along the specified path couples the equations of motion of the rigid body model since all three equations are driven by the same acceleration and speed. The system is therefore indeterminate since it is driven by two control inputs (the front and rear traction forces), of which only one can be determined from the equations of motion.

To resolve this inherent indeterminacy, we add a virtual suspension system that in effect adds two degrees-of-freedom to the system. Adding degrees-of-freedom to the system relaxes the coupling between the three equations of motion, which allows us to solve for the two traction forces required to move the system at the given speed and acceleration along the path.

The vehicle with the suspension is shown in Figure 5. The suspension consists of a linear spring that is free to move along the y body axis. The rear and front springs have a non-compressed length d_0, spring constant k, and compressed lengths d_1 and d_2, respectively. The force applied by a typical spring is thus:

$$P_z = (d_0 - d)k;\ d < d_0. \tag{8}$$

Note that the force applied by the spring is state dependent since d is a function of the vehicle orientation θ. This and the assumption of mass-less wheels allows us to compute an expression that relates the normal force F_n to the traction force F_t.

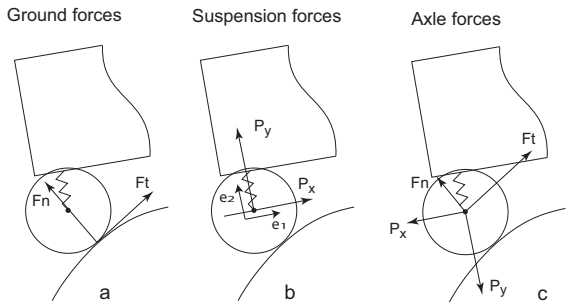

Fig. 3. suspension focus

Figure 3 shows the forces acting on a typical wheel: the ground forces consist of the normal and traction forces F_n and F_t; the suspension applies on the vehicle the forces P_z and P_x; consequently, the forces applied on the axle are F_n, F_t, P_z and P_x. Since the wheels are assumed mass-less, the axle forces must satisfy equilibrium:

$$P_z + F_n n \cdot e_2 + F_t t \cdot e_2 = 0 \tag{9}$$
$$P_x + F_n n \cdot e_1 + F_t t \cdot e_1 = 0, \tag{10}$$

where e_1 and e_2 are the unit vectors in the the suspension coordinates, as shown in Figure 3.

We thus obtained two equations (9-10) in 3 unknowns: P_x, F_n, F_t (P_z is state dependent and hence known). Since we wish to compute the traction force F_t, we first solve for F_n using (9), then substitute it back into the equations of motion (3).

Substituting (8) in (9) and solving for F_n yields:

$$F_n = -aF_t + bP_z. \tag{11}$$

where

$$a = \frac{t \cdot e_2}{n \cdot e_2} \tag{12}$$
$$b = \frac{1}{n \cdot e_2}. \tag{13}$$

For a given P_z, equation (11) expresses F_n as a linear function of F_t. This implies that the ground force $F \in \mathbb{R}^2$ must lie on a straight line that crosses the friction cone, as shown schematically in Figure 4. In effect, this line represents a constraint on the ground force. In contrast, the ground force of the rigid model can span the entire region of the friction cone. The reduction of the ground force to a line enables the direct solution of the inverse dynamics problem.

Substituting the normal forces (11) into the equations of motion (3) yields:

$$F_{t1}(t_1 - a_1 n_1) + F_{t2}(t_2 - a_2 n_2) = m\ddot{x} - b_1 n_1 P_{1z} - b_2 n_2 P_{2z} - mg \tag{14}$$

$$|r_1 \times (F_{t1}(t_1 - a_1 n_1)) + r_2 \times (F_{t2}(t_2 - a_2 n_2))| = I\ddot{\theta} - |r_1 \times b_1 n_1 P_{1z} - r_2 \times b_2 n_2 P_{2z}| \tag{15}$$

where $a_i, b_i, i = 1,2$ are defined in (12,13) for a typical wheel.

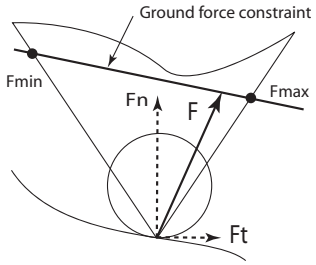

Fig. 4. The friction cone and the ground force constraint

Substituting P_{z1}, P_{z2}, which are state dependent and hence known, in (14-15), yields three equations in the two unknowns F_{t1} and F_{t2}. We use only two of the three equations of motion, usually in X and θ, to solve for F_{t1} and F_{t2} for any given acceleration at a given state. The remaining equation of motion represents the under actuated state.

The two traction forces F_{t1}, F_{t2} are bounded by the upper and lower bounds shown in Figure 4. The extreme points, $F_{min}, F_{max} \in \mathbb{R}^2$ for a typical wheel can be determined analytically using (11) and the equality part of (7) for the lower bound, and (11) and the equality part of (6) for F_{min} and F_{max}, respectively:

$$F_{min} = \begin{bmatrix} F_{nmin} \\ F_{tmin} \end{bmatrix} = \begin{bmatrix} \frac{bP_z}{1-\mu a} \\ -\frac{\mu b P_z}{1-\mu a} \end{bmatrix} \quad (16)$$

$$F_{max} = \begin{bmatrix} F_{nmax} \\ F_{tmax} \end{bmatrix} = \begin{bmatrix} \frac{bP_z}{1+\mu a} \\ \frac{\mu b P_z}{1+\mu a} \end{bmatrix} \quad (17)$$

Note that this derivation applies to an actual suspension, except that we ignored the dumper since it is not needed for the virtual suspension model discussed next.

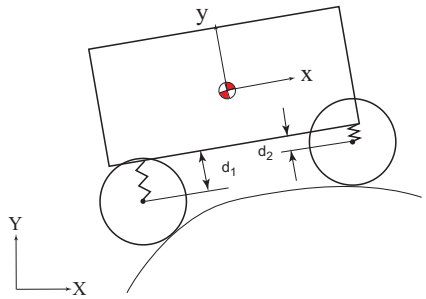

Fig. 5. A planar vehicle model with suspension

V. The Virtual Suspension Model

The virtual suspension model uses equations (14,15), except that the vehicle motion is determined by the rigid body model (1,2). Even though the "rigid suspension" has a constant length, we assume that the longitudinal force P_z is continuous, similarly to the real suspension model. This allows us to compute the traction forces F_{t1}, F_{t2} at a given time step, using the forces P_{z1}, P_{z2} from a previous time step. Once F_{t1}, F_{t2} are computed, P_{z1}, P_{z2} are updated for the next time step.

VI. Examples

The following examples demonstrate our approach to control allocation for a longitudinal vehicle model moving over bumpy terrain. The vehicle parameters, shown in Table I, are of a small dune buggy [13].

A. Example 1: A single bump

Figure 6 shows the bump produced by the exponential function:

$$Z = 0.2e^{-2(x-3)^2} \quad (18)$$

for $x = [0,6]$.

Figure 7 shows the velocity limit curve and the time optimal velocity profile over the bump. The limit curve exhibits two drops, each occurring when one of the wheels passes over the bump. The drop in the velocity profile is caused by the convex nature of the bump, which forces the vehicle to slow down in order to maintain contact with the ground [11]. Also shown in Figure 7 is the time optimal speed profile from rest to rest. It starts with the maximum acceleration, then it slows down to avoid the first drop, then accelerated and slows down again to avoid the second drop, after which is accelerates and decelerates to the final point.

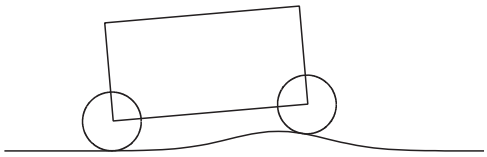

Fig. 6. The bump

mass	589 $[kg]$
Moment of inertia	780 $[kgm^2]$
height of c.g.	0.515 $[m]$
length	2 $[m]$
wheel radius	0.3 $[m]$
coefficient of friction	0.7

TABLE I
Vehicle Data

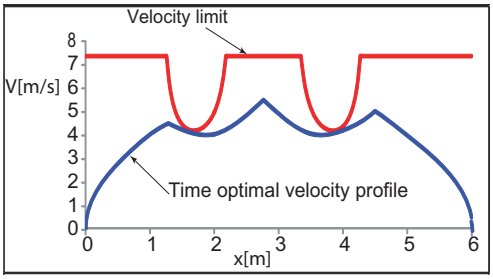

Fig. 7. The time optimal velocity profile over the bump of the all-wheel-drive vehicle

Figures 8 and 9 show (in blue) the ground forces F_{t1} and F_{t2} along the path (18). Also shown (in red) are the upper and lower bounds F_{tmax} (17) and F_{tmin} (16) for each wheel.

The traction forces follow the upper or lower boundaries most of the time, as expected of a time optimal trajectory, except when one of the wheels is close to separating from the ground. This occurs at points where the velocity profile approaches the velocity limit curve, causing the upper and lower bounds to approach zero. That the traction forces do not exceed the upper and lower bounds, verifies the dynamic feasibility of the velocity profile. The normal forces F_{n1} and

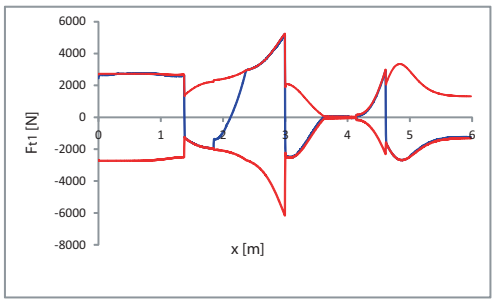

Fig. 8. The rear tangent force (in blue) and the upper and lower bounds

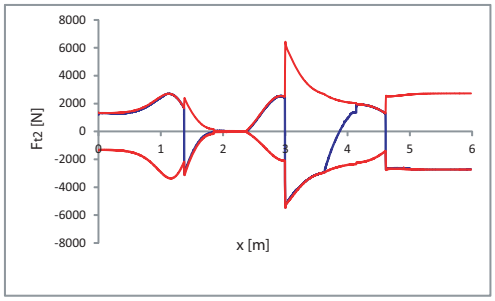

Fig. 9. The front tangent force (in blue) and the upper and lower bounds

F_{n2}, shown in Figures 10,11 are computed by substituting F_{t1}, F_{t2} and P_{z1}, P_{z2} in (11) for each wheel, separately.

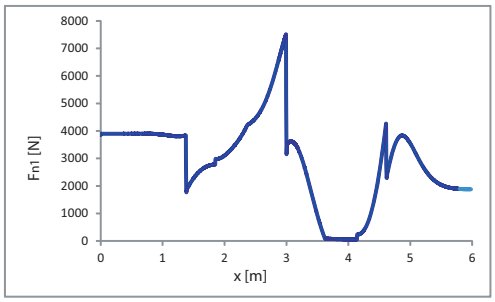

Fig. 10. The normal forces of the rear wheel over the bump

B. Dynamic Simulations

The results of Example 1 were verified by a dynamic simulation of a half vehicle with the parameters shown in Table I and a very stiff spring/damper suspension with a spring constant of $29kN/mm$ and a damping ratio of 0.9. The stiff suspension ensures that the center of mass closely follows the trajectory of the rigid body model. The input to the simulation was the traction forces shown in Figures 8 and

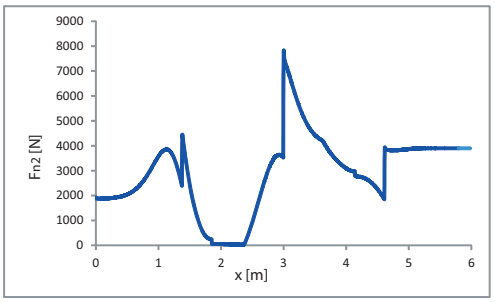

Fig. 11. The normal forces of the front wheel over the bump

9, computed off-line using the virtual suspension model. The suspension forces, P_{z1},P_{z2}, were computed from the actual spring length and its derivative, measured from the vehicle's states:

$$P_z = (d_0 - d)k + c\dot{d};\ d < d_0. \tag{19}$$

The normal forces F_{n1},F_{n2} were then computed from 11. The accelerations $\dot{x}$, $\dot{z}$ and $\dot{\theta}$ were then computed from the equations of motion (3).

The resulting velocity profile is shown in Figure 12. It almost coincides with the optimal velocity profile used to compute the traction forces. Figures 13,14, show the normal rear and front forces, F_{n1} and F_{n2}, respectively. They too are very close to the respective normal forces computed for the rigid body model and shown in Figures 10,11. The simulation results verify that a) the optimal velocity profile is dynamically feasible, b) the wheel torques, allocated by the proposed procedure, do yield the original linear and angular accelerations that when integrated, produce the original velocity profile, and c) the vehicle moves closely to its stability limits (the normal forces are close to zero), as expected from moving along the time optimal velocity profile.

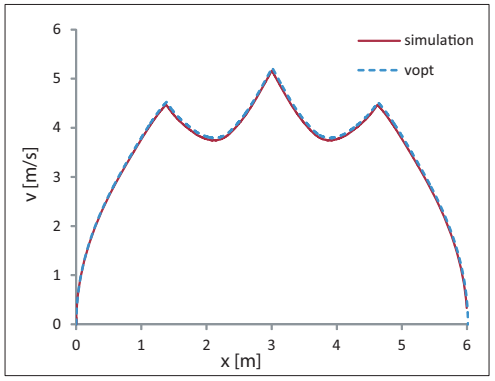

Fig. 12. The optimal and simulated velocity profiles

C. Example 2: Comparison between all-wheel and single-wheel drive

Example 1 was repeated with a front-wheel and rear-wheel drive vehicles of identical parameters. The time optimal velocity profiles for this example are shown in Figures 15,16. The optimal traversal time for the front wheel drive vehicle was $2.49s$, and for the rear-wheel drive vehicle was 2.38,

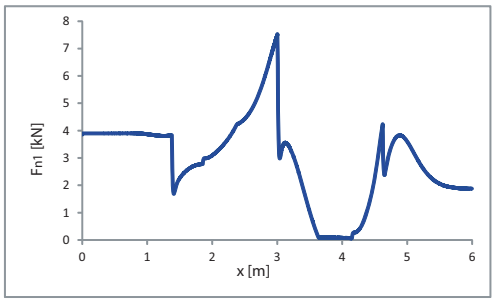

Fig. 13. Simulated normal forces of the rear wheel

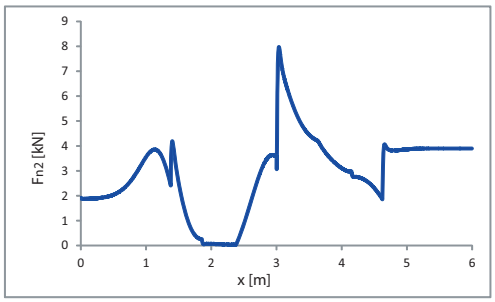

Fig. 14. Simulated normal forces of the front wheel

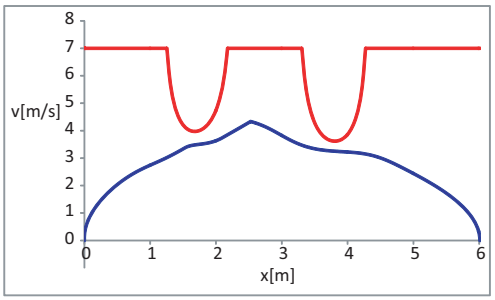

Fig. 15. The time optimal velocity profile over the bump of the rear wheel drive vehicle

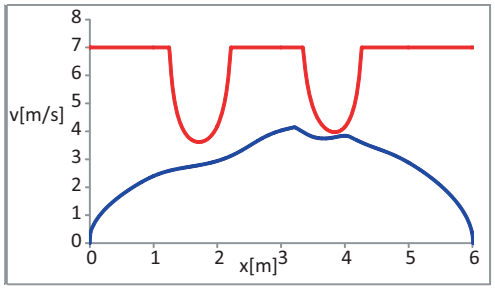

Fig. 16. The time optimal velocity profile over the bump of the front wheel drive vehicle

compared to 2.17s for the all-wheel-drive vehicle. This shows one advantage of the all wheel drive vehicle over a single drive vehicle.

VII. Conclusions

This paper presents a novel approach to computing the individual wheel torques of a planar all wheel drive vehicle that is moving along a specified path at a specified velocity profile. The inverse dynamics problem (computing the wheel torques for a given trajectory) of the indeterminate, or over actuated, system was solved by adding a virtual suspension to the vehicle model. This in effect reduces the number of unknown ground forces, thus allowing for a direct computation of the traction forces at every time step along the path. The end result is driving torques for both wheels that drive the vehicle along the specified trajectory (path and speed). The approach is demonstrated for a planar vehicle moving over rough terrain at the time optimal speeds. The advantage of the all-wheel-drive vehicle was demonstrated by achieving faster velocity profiles than those feasible for the equivalent front and rear wheel drive vehicles. Dynamic simulations verified the proposed approach for control allocation.

References

[1] J.M. Buffington and D.F. Enns. Lyapunov stability analysis of daisy chain control allocation. *Journal of Guidance, Control, and Dynamics*, 19(6):1226 – 30, 1996/11/.

[2] A. Goodarzi and E. Esmailzadeh. Design of a vdc system for all-wheel independent drive vehicles. *Mechatronics, IEEE/ASME Transactions on*, 12(6):632 –639, Dec. 2007.

[3] S.J. Hallowell and L.R. Ray. All-wheel driving using independent torque control of each wheel. In *American Control Conference, 2003. Proceedings of the 2003*, volume 3, pages 2590 – 2595 vol.3, June 2003.

[4] Dongbin Lu, Jianqiu Li, Minggao Ouyang, and Jing Gu. Research on hub motor control of four-wheel drive electric vehicle. In *Vehicle Power and Propulsion Conference (VPPC), 2011 IEEE*, pages 1 –5, Sept. 2011.

[5] N. Mutoh and A. Higashikubo. Electric vehicle system independently driving front and rear wheels. In *IECON 02 [Industrial Electronics Society, IEEE 2002 28th Annual Conference of the]*, volume 2, pages 1386–1391 vol.2, 2002.

[6] N. Mutoh and Y. Takahashi. Front-and-rear-wheel-independent-drive type electric vehicle (frid ev) with the outstanding driving performance suitable for next-generation adavanced evs. In *Vehicle Power and Propulsion Conference, 2009. VPPC '09. IEEE*, pages 1064–1070, 2009.

[7] M.W. Oppenheimer, D.B. Doman, and M.A. Bolender. Control allocation for over-actuated systems. In *Control and Automation, 2006. MED '06. 14th Mediterranean Conference on*, pages 1 –6, June 2006.

[8] Russell P. Osborn and Taehyun Shim. Independent control of all-wheel-drive torque distribution. *Vehicle System Dynamics*, 44(7):529–546, 2006.

[9] J.H. Plumlee, D.M. Bevly, and A.S. Hodel. Control of a ground vehicle using quadratic programming based control allocation techniques. In *American Control Conference, 2004. Proceedings of the 2004*, volume 5, pages 4704 –4709 vol.5, 30 2004-July 2 2004.

[10] Z. Shiller and Y.R. Gwo. Dynamic motion planning of autonomous vehicles. In *IEEE Transactions on Robotics and Automation*, volume 7, pages 241–249, April 1991.

[11] Z. Shiller, M.P. Mann, and D. Rubinstein. Dynamic stability of off-road vehicles considering a longitudinal terramechanics model. In *Robotics and Automation, 2007 IEEE International Conference on*, pages 1170 –1175, April 2007.

[12] F. Tahami, R. Kazemi, and S. Farhanghi. A novel driver assist stability system for all-wheel-drive electric vehicles. *Vehicular Technology, IEEE Transactions on*, 52(3):683 – 692, May 2003.

[13] TOMCAR. http://tomcar.com/wp-content/uploads/2012/tomcar2012.pdf. [accessed 29-July-2013].

[14] Jummin Wang, J.M. Solis, and R.G. Longoria. On the control allocation for coordinated ground vehicle dynamics control systems. In *American Control Conference, 2007. ACC '07*, pages 5724 –5729, July 2007.

[15] Zhiping Zhu, Kui Yuan, Wei Zou, and Huosheng Hu. Current-based wheel slip detection of all-wheel driving vehicle. In *Information and Automation, 2009. ICIA '09. International Conference on*, pages 495 –499, June 2009.